J Wood Sci (2007) 53:463–469
DOI 10.1007/s10086-007-0899-3

ORIGINAL ARTICLE

Kazunari Miyauchi · Koji Murata

Strain-softening behavior of wood under tension perpendicular to the grain

Received: November 10, 2006 / Accepted: April 13, 2007 / Published online: July 8, 2007

Abstract Three softwood samples and one hardwood sample were tested under a tension load applied along the radial direction using small clear specimens and the local tension strain was measured using the digital image correlation method. We successfully obtained a stress–strain curve with a strain-softening branch by calculating the stress using the strain distributions in the vicinity where the specimen ruptured. The continuous digital imaging of the specimen proved to be very effective for measuring the strain in quasi-brittle materials such as wood under tension. The nonlinearity of the stress–strain curve was quantified using two parameters representing the deviation from linear elasticity, and the formula of the stress–strain curve was deduced from the interrelation between these parameters. This formula is expressed quite simply by using the modulus of elasticity along the radial direction and another constant that is unique to the material.

Key words Strain softening · Tension · Digital image correlation · Nonlinearity · Perpendicular to grain

Introduction

Recently, it has been widely recognized that linear elastic theory is not applicable to heterogeneous and quasi-brittle materials such as concrete, ceramics, and wood,[1–3] and that a nonlinear stress–strain curve is required to predict the extent of damage or ultimate fracture. Several studies have investigated the nonlinear stress–strain relationship in the shearing of wood. Okusa[4] and Yoshihara and Ohta[5,6] conducted torsion tests on rectangular cross sections of wooden bars and theoretically examined the shear stress–shear strain relationship in the plastic region. On the other hand, Ukyo and Masuda[7] conducted shear block tests and succeeded in experimentally obtaining the true shear stress–shear strain curves with a strain-softening branch after the peak stress by calculating the shear stress distribution in the shear plane using the shear strain distribution in it.

Although wood under tension that is applied perpendicular to the grain is macroscopically brittle, it is also considered to exhibit a strain-softening behavior. The basis for this conjecture can be attributed to the microscopic fracture and toughening mechanism – microcracking and crack bridging[1,8] – in the vicinity where a specimen will ultimately rupture. However, such a stress–strain curve with a strain-softening branch has never been obtained experimentally for wood under transverse tension; this is because it is difficult to forecast where a specimen would rupture and measure the strain in that location. Therefore, we hypothesized that it might be possible to reveal the mechanical behavior in the vicinity of a rupture if the deformation of the tension test specimen was continuously recorded using a digital video camera and a digital image-analysis technique was applied to measure the strain.

A formula for describing the nonlinear stress–strain relationship is required to precisely simulate the behavior of materials or structural members using numerical analysis, for example, the nonlinear finite element method. In addition, the peak stress can be regarded as the true strength when the stress–strain curve has a softening branch. Typically, the Ramberg–Osgood formula[9] has been used for elastoplastic materials. However, this formula is not useful for predicting the peak stress because of the monotone increasing function of strain. To avoid this shortcoming, O'Halloran proposed a formula that can represent the entire stress–strain curve and remarkably predict the peak stress in wood under compression.[9] However, it is difficult to describe the strain-softening behavior by using this formula.

In this article, we report stress–strain curves with a softening branch in wood subjected to a radial tensile load and

K. Miyauchi (✉) · K. Murata
Division of Forest and Biomaterials Science, Graduate School of Agriculture, Kyoto University, Kitashirakawa Oiwake-cho, Sakyo-ku, Kyoto 606-8502, Japan
Tel. +81-75-753-6236; Fax +81-75-753-6300
e-mail: miyauchi@h1sparc1.kais.kyoto-u.ac.jp

Part of this article was presented at the 56th Annual Meeting of the Japan Wood Research Society, Akita, Japan, August 2006

present a formula describing these curves. We have conceived a method to obtain a formula for the stress–strain curve with a softening branch in terms of the quantification of the nonlinearity of this curve. For quasi-brittle materials such as concrete and ceramics, the degree of brittleness or the nonlinearity of load–displacement or stress–strain curves has been estimated using Hillerborg's characteristic length or the parameters derived from it.[10] Such parameters have also been applied to wood.[11] These parameters are advantageous because they can be easily calculated from the load–displacement or stress–strain curve; however, the shape of the curve cannot be identified by using only one parameter because its value might be similar for different curves. Therefore, in order to overcome this disadvantage, we expressed the nonlinearity of the stress–strain curve using two parameters.

Experimental

Specimen geometry and materials

The shape and dimensions of the tension test specimen were determined in conformance with JIS Z2101. The cross section of the specimen is dumbbell shaped, that is, narrow in the middle like a dumbbell. The details of the specimen geometry are shown in Fig. 1.

JIS Z2101 prescribes three specimen systems: the direction of the tensile load and annual rings must form angles of 0° (T-system), 45° (TR-system), and 90° (R-system), where "T" and "R" indicate the tangential and radial directions, respectively. In this study, the strain was measured over a small area. Thus, the variance of mechanical properties such as the moduli of elasticity in the plane vertical to the loading axis was small for the R-system because this plane was located either in earlywood or latewood. This tendency simplifies the analysis. However, for T- and TR-systems, the plane vertical to the loading axis had stripes of earlywood and latewood; therefore, the variance of mechanical properties in this plane was quite large. Therefore, in this study, the R-system was adopted.

Three softwood samples – spruce (*Picea sp.*), Douglas fir (*Pseudotsuga menziesii*), and hinoki cypress (*Chamaecyparis obtusa*) – and one ring-porous hardwood sample – Japanese oak (*Quercus cuspidata*) – were chosen as specimens. After the specimens were cut, they were conditioned in a climate chamber at a temperature of 20°C and 60% relative humidity for several months. The oven-dry density and moisture content of all the specimens are listed in Table 1.

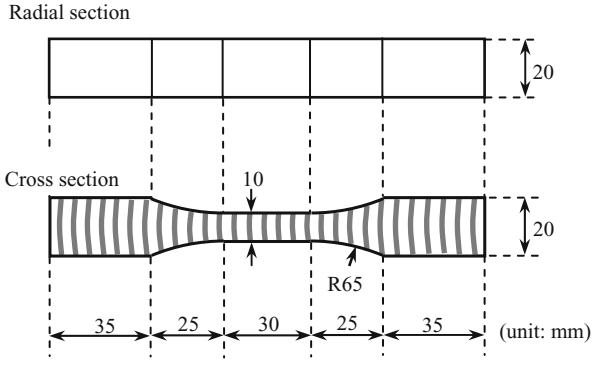

Fig. 1. Japanese Industrial Standard (JIS) tension test specimen

The digital image correlation method (DIC) was used to measure the deformation and calculate the strain in each specimen. The DIC program used in this study was coded by us and it had an accuracy of ±500 microstrains in the standard deviation.[12] The DIC method facilitates the calculation of the displacement vectors of any pixel point in a digital image by means of brightness pattern matching between images, and it requires random patterns of brightness in the images. However, a wood surface has few brightness patterns, and hence the application of DIC to wood is difficult. Consequently, a random dot pattern was generated on the specimen surface by spraying it with black or white water-soluble paint using an airbrush.

Testing method

The jigs holding each end of the tension test specimens to transmit the tensile load were mounted onto a hydraulic servoactuator (Instron; Model 8500) with a static load cell and on the stage of the testing machine. The tensile load was applied under displacement control and recorded at intervals of 1/3 s. The velocity of the crosshead of the testing machine was 0.7 mm/min for spruce and Japanese oak, 0.8 mm/min for Douglas fir, and 1 mm/min for hinoki cypress. These loading conditions were determined such that rupture would occur in approximately 5 min.

In the tension test, the deformation of the specimen was continuously recorded using two digital video cameras (Sony; XCD-SX910). They were set equidistant from the specimen surfaces in order to acquire the images of the middle portion of the cross and radial sections of the specimen (approximately 30 mm along the radial direction). The frame size of the monochrome digital images was 1024 × 768 pixels, and the longer side of the frame coincided with the radial direction of the specimen. Thus, the resolution of the images was approximately 0.03 mm/pixel.

The digital image-capture system (Library; Digital Capture) stores the digital data of the images in a personal computer's temporary memory. Thus, the number of images that can be acquired is determined by the memory capacity of the personal computer and the size of each image. A

Table 1. Properties of specimens

Species	Number of specimens	Density[a] (g/cm^3)	Moisture content (%)
Spruce	22	0.50[b] (5.2)	10.4 (2.2)
Douglas fir	17	0.43 (1.1)	8.8 (2.9)
Hinoki cypress	25	0.33 (0.7)	9.3 (1.3)
Japanese oak	12	0.61 (1.2)	8.5 (1.3)

[a] Oven-dry density
[b] Data given as means with coefficient of variation in percent given in parentheses

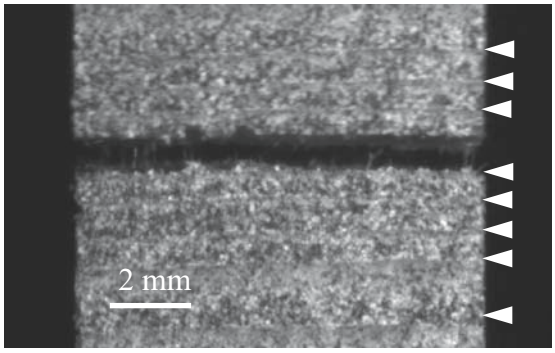

Fig. 2. Ruptured spruce specimen. *Arrowheads* indicate the annual ring boundaries

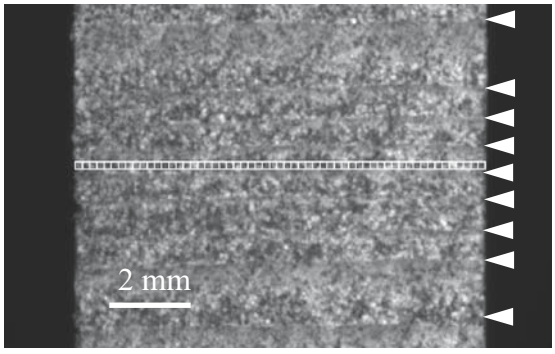

Fig. 3. Digital image correlation (DIC) elements in the reference image

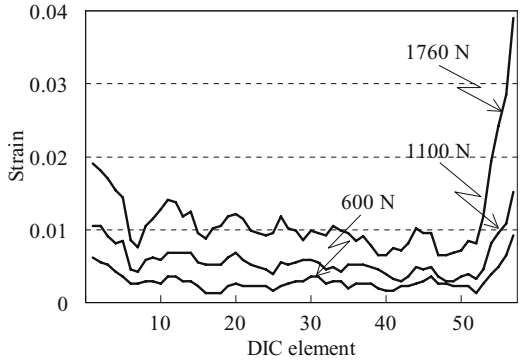

Fig. 4. Distributions of the radial tensile strain measured on the cross-sectional image of a spruce specimen

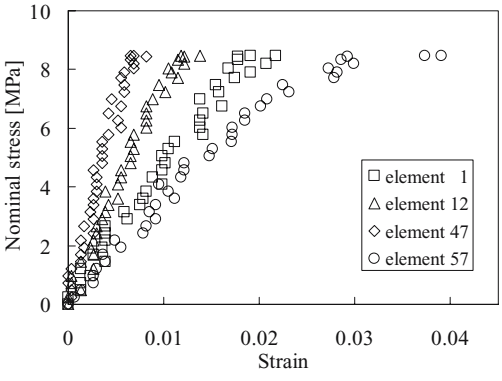

Fig. 5. Relationships between the nominal stress and strain

Windows XP system can store 2 gigabytes of data in temporary memory and the size of each image would be approximately 8 kilobytes; thus, a little more than 1000 images could be stored in each camera. Because the images were captured at intervals of 1/3 s, the deformation of the specimen could be recorded for 6 min.

Strain measurement using DIC

As shown in Fig. 2, the tensile load along the radial direction caused the rupture of the specimen at the earlywood in an annual ring, which is the weakest layer in the specimen. Japanese oak, which is a ring-porous wood, ruptured at a pore zone. Therefore, we hypothesized that the largest radial tensile strain could occur in this weakest layer and that we would be able to obtain the stress–strain curve with a strain-softening branch after the peak stress by investigating the deformation behavior in this layer.

The tensile strain along the radial direction was calculated using DIC. In the reference digital image, in which no deformation was observed before loading, a DIC analysis field consisting of aligned elements was established at the region where the rupture would occur (Fig. 3). The number of elements was approximately 55 and 110 for the cross-section and radial-section images, respectively. The strain in an element was calculated by measuring the displacement vectors of the four nodes that constitute the element.

If all the images had been used for DIC, the analysis would have required a large amount of time because approximately 800 images were obtained from each camera during a single tension test. Thus, 1 image captured just before the occurrence of rupture and 39 images captured at regular intervals under the applied tensile load were selected.

Results and discussion

Redistribution of tensile load

An example of the distribution of the radial tensile strain obtained using the DIC analysis is shown in Fig. 4. From this figure, it is evident that the strain was not uniformly distributed in the earlywood of the specimen and that a considerably large tensile strain was concentrated in a narrow area. In addition, it is also assumed that the ultimate fracture originated from this area. The wide strain distribution can be ascribed to the fact that the tensile forces present in the elements for DIC were not equal. If this fact is neglected or if it is assumed that the tensile forces all over the elements are uniform, which implies that the nominal stress corresponds to the strain of each element, the stress–strain relationships of all the elements are not found to be unique, as shown in Fig. 5. Thus, in order to obtain a unique relation-

ship between the stress and strain, the tensile force in an element must be calculated by employing the redistribution of the tensile load following the straining of each element.[7] Using this method, the stress can be calculated as follows:

$$\sigma_i = \frac{P \cdot f(\varepsilon_i)}{\sum_{i=1}^{N} \{f(\varepsilon_i) \cdot A_i\}}, \quad (1)$$

where σ and ε are the stress and strain along the radial direction, respectively; P, the tensile load; N, the number of elements or divisions in the transverse section; A, the area subjected to the tensile force; $f(\varepsilon)$, a weighting function; and index i denotes the ith element. When the sizes of the elements are constant, A_i equals A/N, and Eq. 1 can be rewritten as follows:

$$\sigma_i = \frac{P}{A} \cdot \frac{f(\varepsilon_i)}{\frac{1}{N}\sum_{i=1}^{N} f(\varepsilon_i)} = \bar{\sigma} \cdot \frac{f(\varepsilon_i)}{\bar{f}(\varepsilon)}, \quad (2)$$

where $\bar{\sigma}$ is the nominal stress and $\bar{f}(\varepsilon)$ is the average of $f(\varepsilon_i)$.

The concern emerging here is the determination of the appropriate weighting function to be used to distribute the tensile load. The relationship between the stress and strain can be used as a weighting function; therefore, if the stress–strain relationship is linear, we can simply substitute $f(\varepsilon_i)$ with ε_i in Eq. 1. However, it is clear that this assumption is not applicable because of the nonlinear relationship between the stress and strain (Fig. 5). Hence, the tensile load must be redistributed using a nonlinear weighting function, which is not yet known. Therefore, we corrected a weighting function iteratively and then obtained a single stress–strain curve. The procedure involved in this method is as follows. First, the stress–strain relationship of the element where the maximum tensile strain occurred was extracted and fitted using a three-dimensional smoothing spline curve. Second, the weighting function $f(\varepsilon)$ in Eq. 1 was substituted with the smoothed curve and the stress was corrected. These two steps were iterated until all the stress–strain relationships converged onto a single curve. The flow for calculating the stress–strain curve is shown in Fig. 6. In this diagram, the fifth step of the algorithm is required to exclude an impossible form of the stress–strain curve and to avoid the stress divergence during the iterative correction.

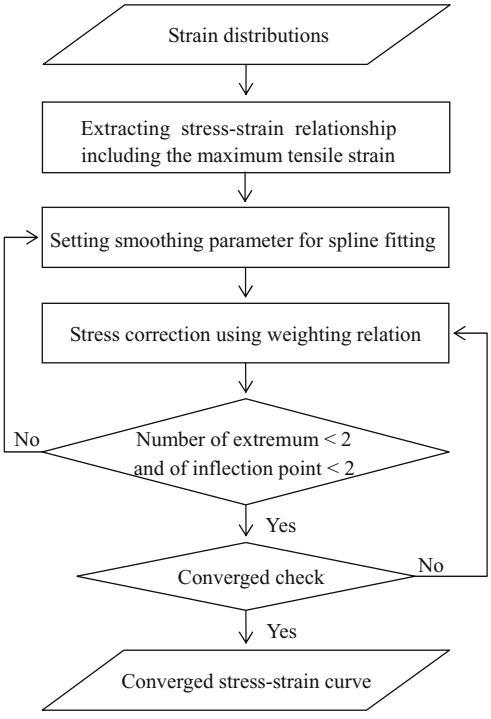

Fig. 6. Flowchart of stress–strain curve calculation

Strain-softening behavior

Examples of the stress–strain curves modified by redistributing the tensile load are shown in Fig. 7. Two solid curves in each graph were obtained from the strain distributions of the cross and radial sections of the same specimen, and the broken line represents the nominal tensile strength σ_{nom} calculated by dividing the maximum tensile load by the initial area of the ruptured region. Because the tensile stress acting on the transverse section of the specimen was not uniform, the maximum strains measured on both sections were not necessarily equal. Of all the stress–strain curves, 47% exhibited strain-softening behavior and their peak stresses were attained at the following tensile strain ranges: Japanese oak, 0.021 ± 0.003; spruce, 0.024 ± 0.004; hinoki cypress, 0.030 ± 0.006; and Douglas fir, 0.033.

The ratio of the maximum stress σ_{max} obtained from the stress–strain curve to the nominal tensile strength is listed in Table 2. The ratios for cross and radial sections were as follows: spruce, 1.43 ± 0.20 and 1.44 ± 0.18; Douglas fir, 1.36 ± 0.16 and 1.46 ± 0.22; hinoki cypress, 1.58 ± 0.24 and 1.27 ± 0.11; and Japanese oak, 1.28 ± 0.16 and 1.25 ± 0.16. On the basis of the Douglas fir example shown in Fig. 7, a lower maximum tensile strain exhibited the tendency to yield a more linear stress–strain curve and a larger maximum stress as compared with a higher maximum tensile strain yielding a stress–strain curve with a softening branch. This suggests that only when the strain softening appears, the maximum stress, which is equal to the peak stress in this case, can adequately approximate the true tensile strength.

The strain-softening behavior and fracture mechanism are closely related to each other when the tension is applied perpendicular to the grain. When an undamaged specimen is subjected to radial tensile stress, the specimen is subjected to strain, and microcracks begin to grow from the microscopic defects that inherently exist in cell walls and cell boundaries; this is followed by the occurrence of new microscopic defects. This damage is scattered throughout the system and uniformly decreases the capability of the system to transmit the tensile load or increases the compliance of the system. Consequently, the stress–strain curve deviates from linear elasticity and bends over. Moreover, the system remains stable as long as the elastic strain energy absorbed in the system increases, even if the stress begins

Table 2. Ratio of maximum stress to nominal strength

Species	Cross section				Radial section			
	n	σ_{max} (MPa)	σ_{nom} (MPa)	$\sigma_{max}/\sigma_{nom}$	*n*	σ_{max} (MPa)	σ_{nom} (MPa)	$\sigma_{max}/\sigma_{nom}$
Spruce	16 (7)	12.4 ± 1.8	8.7 ± 0.9	1.43 ± 0.20	16 (7)	12.4 ± 1.2	8.7 ± 0.9	1.44 ± 0.18
Douglas fir	4 (0)	12.3 ± 1.2	9.1 ± 0.2	1.36 ± 0.16	4 (1)	13.2 ± 1.7	9.1 ± 0.2	1.46 ± 0.22
Hinoki cypress	7 (2)	11.8 ± 2.0	7.5 ± 0.1	1.58 ± 0.24	7 (3)	9.5 ± 0.9	7.5 ± 0.1	1.27 ± 0.11
Japanese oak	9 (6)	16.8 ± 2.1	12.9 ± 1.1	1.28 ± 0.16	10 (8)	16.1 ± 2.2	12.9 ± 1.1	1.25 ± 0.16

n, Number of stress–strain curves and numbers in parentheses indicate those exhibiting strain-softening behavior; σ_{max}, maximum stress; σ_{nom}, nominal strength

Fig. 7. Examples of stress–strain curves

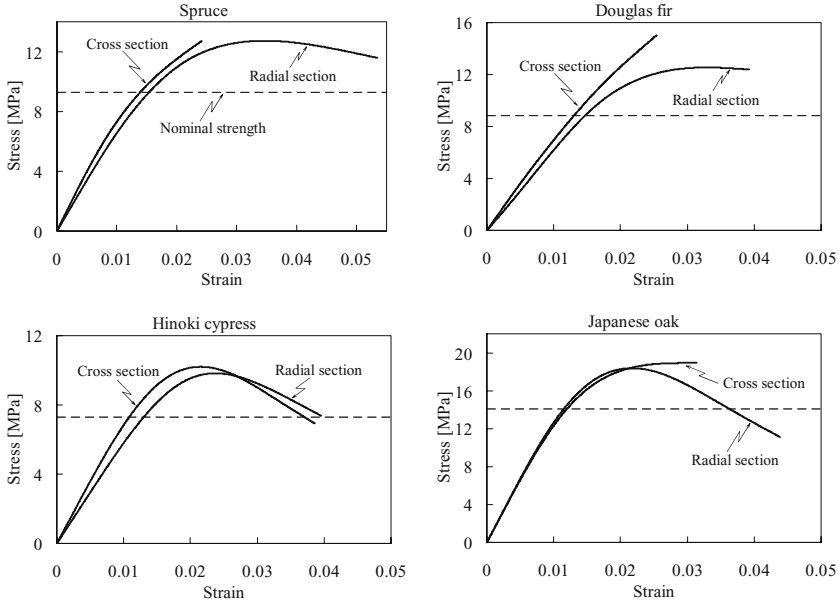

to decline. An increase in the tensile strain results in intercellular separation or intracellular fracture, thereby forming a localized critical crack surface.[8] Although this localized fracture increases compliance, the elastic strain energy absorbed in the system decreases because the effective ligament that transmits the tensile load decreases. Therefore, the system becomes unstable. Here, it should be noted that the microcracking and the propagation of the critical crack are not exclusive but simultaneous, and predominance changes gradually from the former to the latter with the increase in strain.

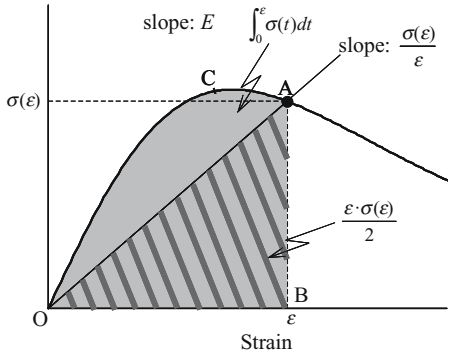

Fig. 8. Schematic diagram of nonlinearity of a stress–strain curve. The reciprocal of E is the initial compliance of a material and that of $\sigma(\varepsilon)/\varepsilon$ is the compliance at strain ε. The area of OCAB and OAB correspond to the strain energy density and the elastic strain energy density at strain ε, respectively

Formula for stress–strain curves

We expressed the nonlinearity of the stress–strain curve using two parameters – $u(\varepsilon)$ and $v(\varepsilon)$ – in order to obtain a formula for the stress–strain curve with a softening branch. These parameters were defined as follows:

$$u(\varepsilon)=\frac{\sigma(\varepsilon)}{E_R\cdot\varepsilon},\quad v(\varepsilon)=\frac{\varepsilon\cdot\sigma(\varepsilon)}{2\int_0^\varepsilon\sigma(t)dt},\tag{3}$$

where E_R is the modulus of elasticity along the radial direction. As shown in Fig. 8, $u(\varepsilon)$ is the ratio of the stiffness at ε to the initial stiffness, and $v(\varepsilon)$ is the ratio of the elastic strain energy density – area of OAB – to the strain energy density – area of OCAB – at ε. The values of these parameters range from zero to unity. If the materials exhibit linear elasticity, the values are unity; these values decrease with the degree of nonlinearity of the stress–strain curve. In order to characterize the nonlinearity of the stress–strain curve, we assumed, for convenience, that no plastic strain

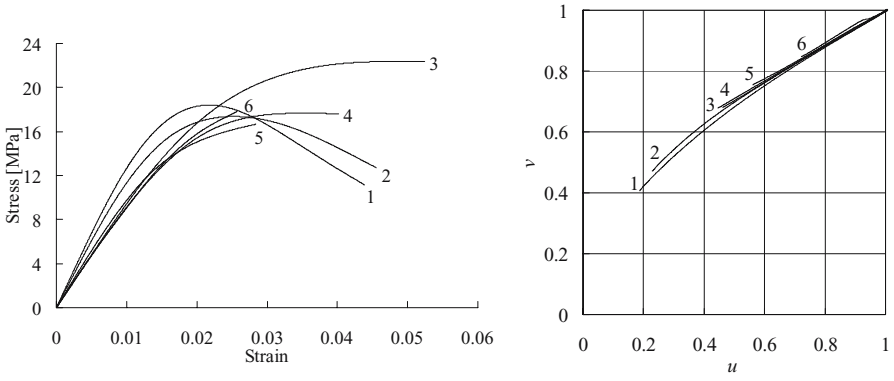

Fig. 9. Stress–strain and *u*-*v* relationships of Japanese oak

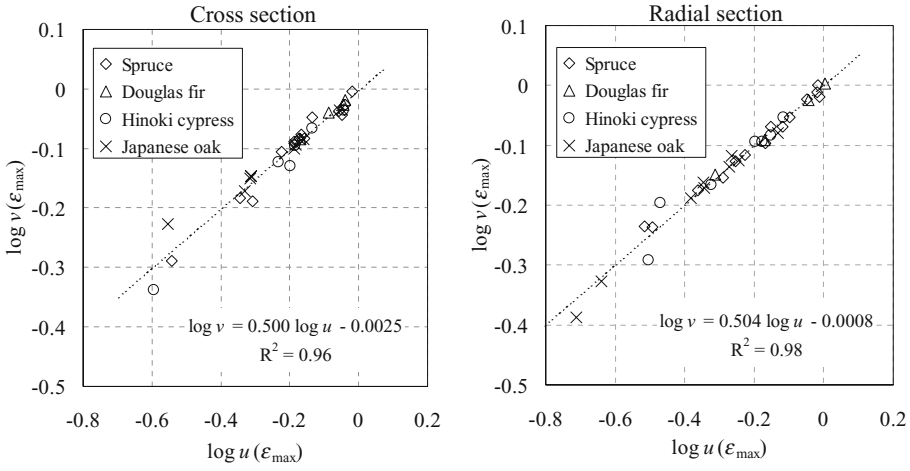

Fig. 10. Double logarithmic relationships between *u* and *v* at maximum strain

was present. Nevertheless, this assumption is appropriate because, as mentioned in the previous section, the main cause of the nonlinearity in the stress–strain relationship is the decrease in the load transmission capability by the accumulation of microscopic fracture and the propagation of the critical crack; moreover, the undamaged region shows elastic behavior.

Some stress–strain curves with various nonlinearities and the corresponding *u*-*v* curves are shown in Fig. 9. The *u*-*v* curves converge on the same curvature despite the varying shapes of the stress–strain curves. This indicates that the fracture process is common to all the specimens and that all tensile stress–strain curves can be expressed by using a single formula.

In order to obtain the formula, the relationship between *u* and *v* was investigated. *u* and *v* at the maximum strain ε_{max} were calculated as the representative values for all the stress–strain curves. As shown in Fig. 10, the *u*-*v* relationship was linear under a double logarithm and the gradient was 0.5, independent of the wood species. Therefore, the relationship between *u* and *v* could be expressed as an exponential function as follows:

$$v(\varepsilon) = u(\varepsilon)^{0.5}. \tag{4}$$

The formula for the stress–strain curves when the tension is applied perpendicular to the grain can be obtained by substituting Eq. 3 in Eq. 4 and then solving the resulting equation. The stress–strain curve is expressed quite simply as follows:

$$\sigma(\varepsilon) = \frac{E_R \cdot \varepsilon}{\left\{1 + \left(\frac{\varepsilon}{\varepsilon_{inflect}}\right)^2\right\}^2}, \tag{5}$$

where $\varepsilon_{inflect}$ is an integration constant and corresponds to the strain at the inflection point of the stress–strain curve. In Eq. 5, the numerator represents linear elasticity and the denominator represents nonlinearity or the rate of increase in compliance, and it has a more significant effect on the stress with a change in the strain. In addition, the estimation of the true tensile strength along the radial direction, $\sigma_{strength}$, is expressed as follows:

$$\sigma_{strength} = \frac{3\sqrt{3}}{16} E_R \cdot \varepsilon_{inflect}. \tag{6}$$

The elastic strain energy density absorbed in the system, which corresponds to the area of OAB in Fig. 8, increases when $\varepsilon < \varepsilon_{inflect}$ and decreases when $\varepsilon_{inflect} < \varepsilon$; that is, it is a maximum at $\varepsilon = \varepsilon_{inflect}$, because no plastic strain is assumed. Hence, the main fracture mechanism changes from microcracking to the propagation of the critical crack at $\varepsilon = \varepsilon_{inflect}$ and the system becomes unstable. Therefore, $\varepsilon_{inflect}$ can be

regarded as a constant that is unique to each material characterizing the behavior of the deformation or fracture of wood.

Although Eq. 5 is based on the behavior of earlywood along the radial direction, this formula can be applied to latewood as well. We believe that further studies are required to confirm this.

Conclusions

We conducted tension tests along the radial direction of wood and investigated the relationship between the stress and strain. Stress–strain curves with a strain-softening branch were obtained by calculating the stress using the strain distributions in the vicinity where the specimens ruptured. The peak stresses were achieved at a tensile strain of 0.02–0.03. The nonlinearity of the stress–strain curve was quantified using two parameters representing the deviation from linear elasticity. The formula for the stress–strain curve was deduced from the interrelation between these parameters. This formula is expressed quite simply using the modulus of elasticity along the radial direction and another constant unique to the material.

References

1. Vasic S, Smith I (2002) Bridging crack model for fracture of spruce. Eng Fract Mech 69:745–760
2. Stanzl-Tschegg SE, Tan DM, Tschegg EK (1995) New splitting method for wood fracture characterization. Wood Sci Technol 29:31–50
3. Tschegg EK, Frühmann K, Stanzl-Tschegg SE (2001) Damage and fracture mechanisms during mode I and mode III loading of wood. Holzforschung 55:525–533
4. Okusa K (1977) On the prismatical bar torsion of wood as elastic and plastic material with orthogonal anisotropy (in Japanese). Mokuzai Gakkaishi 23:217–227
5. Yoshihara H, Ohta M (1995) Shear stress–shear strain relationship of wood in the plastic region. Mokuzai Gakkaishi 41:529–536
6. Yoshihara H, Ohta M (1995) Determination of the shear stress–shear strain relationship of wood by torsion tests. Mokuzai Gakkaishi 41:988–993
7. Ukyo S, Masuda M (2004) Investigation of the true stress–strain relation in shear using the digital image correlation method (in Japanese). Mokuzai Gakkaishi 50:146–150
8. Smith I, Landis E, Gong M (2003) Fracture and fatigue in wood. Wiley, Chichester, pp 99–121
9. Bodig J, Jayne BA (1982) Mechanics of wood and wood composites. Van Nostrand Reinhold, New York, pp 285–290
10. Harmuth H, Rieder K, Krobath M, Tschegg E (1996) Investigation of the nonlinear fracture behaviour of ordinary ceramic refractory materials. Mater Sci Eng A214:53–61
11. Reiterer A, Sinn G, Stanzl-Tschegg SE (2002) Fracture characteristics of different wood species under mode I loading perpendicular to the grain. Mater Sci Eng A332:29–36
12. Murata K, Masuda M, Ukyo S (2005) Analysis of strain distribution of wood using digital image correlation method – four-point bend test of timber including knots (in Japanese). Trans Visualiz Soc Jpn 25:57–63